PCCP

ROYAL SOCIETY OF CHEMISTRY

PAPER

View Article Online
View Journal | View Issue

Cite this: *Phys. Chem. Chem. Phys.*, 2024, **26**, 15891

Synergistic effect of adsorption-photocatalytic reduction of Cr(VI) in wastewater with biochar/TiO_2 composite under simulated sunlight illumination†

Yadong Du,[ab] Xiangju Ye,*[b] Zhenzhen Hui,[b] Die Jiao,[a] Yue Xie,*[a] Shifu Chen*[c] and Jun Ding[d]

Received 23rd March 2024,
Accepted 29th April 2024

DOI: 10.1039/d4cp01226g

rsc.li/pccp

Photocatalysis, which is an alternative technology to conventional methods, utilizes solar energy as the driving force to address environmental concerns and has attracted widespread attention from chemists worldwide. In this study, a series of photocatalytic materials composed of agricultural waste and titanium dioxide (TiO_2) nanomaterial was prepared for the synergistic adsorption-photocatalytic reduction of hexavalent chromium in wastewater under mild conditions. The results showed that the TiO_2 nanomaterial exhibited a higher photogenerated carrier separation efficiency and performance for the adsorption-photocatalytic reduction of Cr(VI) after loading straw biochar (BC). When the loading amount of BC was 0.025 g (*i.e.*, TBC-3), the removal efficiency of Cr(VI) was as high as 99.9% under sunlight irradiation for 25 min, which was 2.9 and 3.5 times higher than that of pure TiO_2 and BC samples, respectively. Additionally, after four cycles of experiments, the removal efficiency of Cr(VI) by TBC-3 remained at about 93.0%, proving its good chemical ability in our reaction system. Its excellent adsorption-photocatalytic performance is mainly attributed to the synergistic effect of the strong adsorption of BC and the outstanding photocatalytic performance of TiO_2. Finally, the possible mechanism for the synergistic adsorption-photocatalytic reduction on BC/TiO_2 to remove the highly toxic Cr(VI) in wastewater was proposed.

1. Introduction

Presently, the rapid industrialization has resulted in increasing water pollution with various heavy metal pollutants. Among the heavy metal ions, hexavalent chromium [Cr(VI)] in wastewater is a well-known and widespread toxic pollutant, which has become a serious threat to human health and the environment.[1–3] Currently, Cr(VI) is extensively used in industrial processes, including electroplating, tanning, metallurgy, dyes and wastewater treatment, leading to the production of a large amount of corresponding by-product wastewater.[2,4–6] Thus, considerable research efforts have been devoted to developing methods for the removal of Cr(VI) from industrial wastewater, including chemical precipitation method,[7,8] ion exchange method,[9–11] and membrane separation method.[12–16] However, the drawbacks of the above-mentioned technologies, such as low efficiency, high cost, high energy consumption, and significant by-product pollution, seriously restrict their practical applications.[17] Therefore, it is of great significance to develop efficient, economical and environmentally friendly technology for the removal of Cr(VI) from wastewater.[18,19]

In recent years, photocatalytic technology has attracted significant attention as a potential environmental remediation method.[20–23] Photocatalysis can fully use solar energy to reduce Cr(VI) to trivalent chromium [Cr(III)] in wastewater.[24,25] To date, numerous photocatalysts such as Fe_{NPs}@Fe_{SAs}NC, $ZnIn_2S_4$/CdS, CoO@$MnCo_2O_4$, and CeO_2/BiOX have been developed.[26–29] Among these, titanium dioxide (TiO_2) has received considerable attention due to its excellent photocatalytic performance.[30,31] However, TiO_2 is associated with many limitations in the photocatalytic process, such as high recombination rate of photogenerated electron–hole pairs, which seriously affect its widespread applications.[32] Thus, to overcome the above-mentioned problems,

[a] *College of Resources and Environment, Anhui Science and Technology University, Fengyang, Anhui 233100, P. R. China. E-mail: yorke@126.com; Fax: +86-561-3802000; Tel: +86-561-3802000*
[b] *College of Chemistry and Materials Engineering, Anhui Science and Technology University, Bengbu, Anhui 233030, P. R. China. E-mail: yexiangju555@126.com*
[c] *College of Chemistry and Materials Science, Huaibei Normal University, Huaibei, 235000, P. R. China. E-mail: chshifu@chnu.edu.cn*
[d] *Anhui Haohong Biotechnology Co., Ltd, Hefei, Anhui 230026, P. R. China*
† Electronic supplementary information (ESI) available. See DOI: https://doi.org/10.1039/d4cp01226g

one of the most effective strategies is to design and develop novel composite materials.[33–35]

As a porous material with a high specific surface area, BC exhibits numerous potential applications in the fields of adsorption and catalysis.[36,37] BC can be prepared *via* the pyrolysis or coking of low-cost and wide-source agricultural biomass waste such as straw and sawdust.[38] Due to its unique structure and outstanding chemical properties, BC has excellent adsorption property and can be used to remove organic and inorganic pollutants.[39] More importantly, the surface of BC can be modified or mixed with catalytic materials, which can be employed to fabricate excellent photocatalytic composite materials.[36,40] Therefore, BC/TiO_2 composite materials can be developed to synergistically adsorb and photocatalytically reduce Cr(VI) to Cr(III) in wastewater. Herein, BC, due to its high specific surface area and abundant functional groups, was employed as a platform to adsorb Cr(VI) in wastewater for subsequent reactions. TiO_2 as a photocatalyst can reduce the Cr(VI) adsorbed by BC into non-toxic Cr(III) with photogenerated carriers. Meanwhile, BC, as a good electron acceptor, can accelerate the separation of the photogenerated carriers in TiO_2, thus improving the efficiency of the adsorption-photocatalytic reaction.[41–43] However, the photocatalytic reduction effect and mechanism for the reduction of Cr(VI) to non-toxic Cr(III) using straw biochar-based composite samples have been rarely reported to date.

Straw biochar and titanium dioxide nanocomposite photocatalytic materials were fabricated *via* a multiple-calcination method, and the adsorption-photocatalytic performance of the as-synthesized composite materials was investigated by the removal of Cr(VI) in wastewater under sunlight irradiation. The results indicated that the adsorption-photocatalytic activity of the TBC composites for the removal of Cr(VI) significantly increased compared with the TiO_2 and BC samples and the adsorption-photocatalytic activity increased, and then decreased with an increase in the loading amount of BC. The optimal loading amount of BC was determined to 0.025 g (*i.e.* TBC-3), which exhibited a removal efficiency of *ca.* 2.9- and 3.5-times higher than that of the pure TiO_2 and BC samples, respectively. Furthermore, the chemical stability of TBC-3 was also proven after the four runs of cyclic experiments. The outstanding remove efficiency of Cr(VI) by the TBC composites is ascribed to the synergistic effect of the adsorption-photocatalytic reaction. The aim of this work was to develop a new and efficient biochar-based composite material, which has potential applications in the treatment of highly toxic chromium-containing wastewater.

2. Experimental

2.1. Preparation of BC

Wheat straw (self-made in our laboratory) was ultrasonically washed with deionized water, dried at 65 °C for 24 h, broken by a wall-breaking machine and sieved with a 100 mesh. Subsequently, the powder was transferred to a muffle furnace, and then heated to 500 °C for 2 h at a heating rate of 5 °C min^{-1}. The prepared sample was collected after naturally cooling to room temperature. Finally, the obtained BC was acidified with 1 M hydrochloric acid for 2 h, washed with deionized water to neutral, and then dried at 65 °C overnight.

2.2. Preparation of BC/TiO_2 composite material

10 mL tetrabutyl titanate, 40 mL anhydrous ethanol, 4 mL of deionized water and 1 mL of acetic acid were magnetically stirred for 30 min, obtaining a transparent solution. Subsequently, 0.100, 0.050, 0.025, 0.010 and 0.001 g acidified biochar were added to the above-mentioned mixed solution under vigorous stirring, respectively. The mixture was aged for 24 h, centrifuged and dried at 65 °C for 12 h. Finally, the black precipitate was transferred to a muffle furnace and heated to a certain temperature for 2 h at a heating rate of 5 °C min^{-1}. The composite samples were obtained and labeled as TBC-*X* (*X* represents the weight of BC. For example, *X* = 1, 2, 3, 4 and 5 represent 0.100, 0.050, 0.025, 0.010 and 0.001 g biochar stand, respectively). Titanium dioxide was prepared using the same procedure in the absence of BC.

2.3. Photocatalytic activity measurements

The synergistic adsorption-photocatalytic reduction of Cr(VI) with the as-obtained samples under simulated sunlight irradiation was evaluated. Typically, 100 mg photocatalyst was dispersed in 100 mL simulated Cr(VI) wastewater solution (10 ppm) with a pH of 3.1, and then 1 mM methanol was added as a hole sacrificial agent. The solution was stirred in the dark for 30 min to establish the adsorption–desorption equilibrium of Cr(VI) on the surface of the sample. After sunlight irradiation (a full-spectrum Xenon lamp with a light intensity of 900 mW cm^{-2} and an irradiation area of 80 cm^2 were used for photocatalytic testing to simulate sunlight), 2 mL aqueous solution was sampled at fixed intervals during the reaction and filtered using a 0.22 μm filter membrane. The concentration of Cr(VI) was determined by a colorimetric titration method based on the formation of the pink-colored complex Cr(VI)-diphenylcarbazide using a UV-Vis spectrophotometer at 540 nm.[44] The reaction system was maintained at room temperature using a constant temperature cooling tank and a CEL-HXF300E7 (Beijing China Education Au-light Co., Ltd) was used as the simulated light source.

3. Results and discussion

3.1. Characterization

3.1.1. XRD. The crystallographic structures of BC, TiO_2 and BC/TiO_2 composite samples were analyzed by XRD, and the results are shown in Fig. 1. Diffraction peaks corresponding to the crystal planes of (101), (004), (200), (105), (211), (204), (116), (220), (215) and (224) were observed, which are assigned to the crystallographic planes of anatase phase TiO_2 (JCPDS file no. 021-1272).[45] Moreover, the samples with different loading amounts of BC showed obvious peak broadening, which is

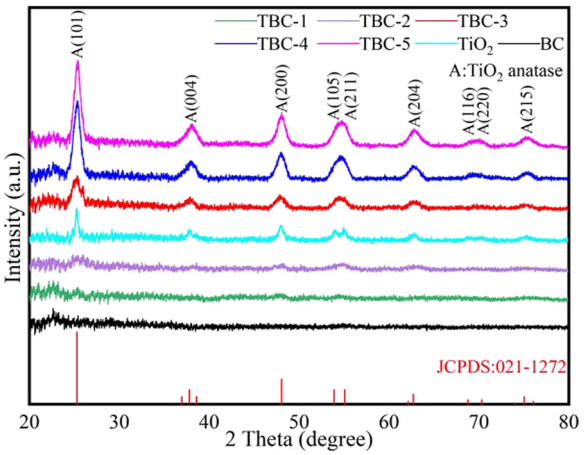

Fig. 1 XRD patterns of BC, TiO_2 and TBC samples.

possibly because of the formation of a smaller grain size in the TBC composites compared with TiO_2.[46] As shown in Fig. 1, when the loading amount of BC was less than 0.01 g, the intensity of the anatase diffraction peak of TiO_2 increased, whereas when the loading amount of BC was higher than 0.01 g, the intensity of the diffraction peak significantly decreased. This implies that an excess loading of biochar inhibits the growth of TiO_2 crystals or disrupt their structural arrangement.[35] The d spacing of TiO_2, TBC-1, TBC-2, TBC-3, TBC-4 and TBC-5 calculated using Bragg's law ($n\lambda = 2d_{hkl}\sin\theta$) was 3.7, 3.5, 3.6, 3.6, 3.7 and 3.7 Å, respectively, which is consistent with the TEM result (d = 0.357 nm). This demonstrates that TBC was successfully synthesized employed our synthetic method.

3.1.2. XPS. X-ray photoelectron spectroscopy (XPS) was employed to determine the element compositions and chemical states of the as-prepared samples, as shown in Fig. 2. It can be found in Fig. 2a that the composite photocatalyst mainly contained Ti, O and C elements. Further investigation indicated that the peaks located at the binding energies of 459.4 and 465.1 eV with a spin–orbit splitting energy of 5.7 eV can be ascribed to Ti ($2p_{1/2}$) and Ti ($2p_{3/2}$) of Ti^{4+} in the anatase phase TiO_2 (Fig. 2b), respectively. Furthermore, the oxygen spectrum of the composite exhibited two peaks located at 530.7 and 532.4 eV, corresponding to the Ti–O–Ti bond of O^{2-} in the TiO_2 sample and the C–O bond and C–OH group band in the acidified biochar materials, respectively. It is noteworthy that the slight shift in binding energy for the Ti–O–Ti bond in the O 1s spectrum may be due to the presence of a small amount of non-lattice oxygen (Fig. 2c).[24] Importantly, the C 1s spectrum could be deconvoluted into four peaks with binding energies of 287.0, 289.5, 284.8 and 285.7 eV. Among them, the former two peaks correspond to O=C–O and C–O, while the latter two represent the C–C peaks of sp^2 and sp^3 hybrid C atoms in the carbonaceous material, respectively.[47]

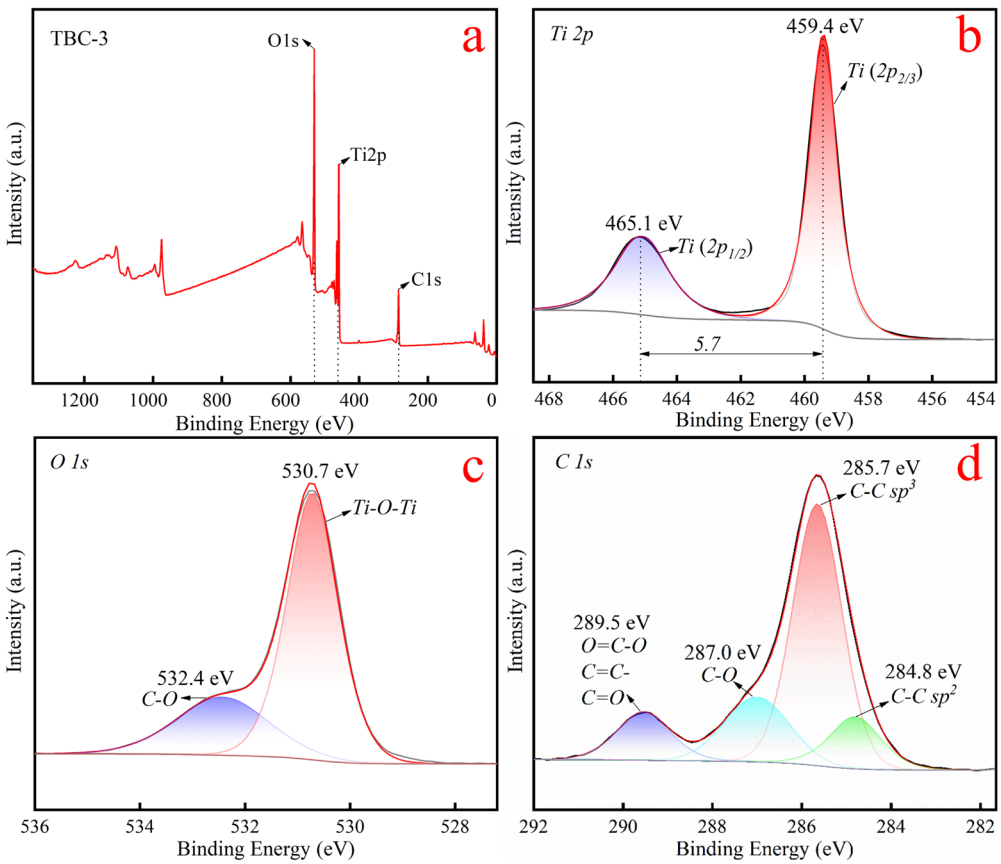

Fig. 2 XPS survey patterns of TBC-3 (a). High-resolution XPS spectra of Ti 2p (b), O 1s (c) and C 1s (d).

Notably, no peak of C–Ti bond was detected near 281.5 eV, implying that there is no C–Ti bond in the composite material between the BC and TiO_2 samples.[24]

3.1.3. UV-Vis absorption spectra. The UV-Vis absorption spectra of the prepared TiO_2 and series of composite samples were studied in the wavelength range of 200–800 nm, and the obtained spectra are shown in Fig. 3. It can be observed that all the samples exhibit a typical anatase absorption edge at around 360 nm, which suggests that the as-prepared TiO_2 is a potentially excellent UV light-responsive photocatalyst. Moreover, the incorporation of BC in the matrix TiO_2 has an obvious influence on the optical properties of light absorption in the TBC composite. Based on the UV-Vis diffuse reflectance, the band gap energy values of TiO_2, TBC-1, TBC-2, TBC-3, TBC-4 and TBC-5 were determined to be 3.65, 3.43, 3.41, 3.39, 3.64 and 3.62 eV, respectively, which indicate that the band gap of TBC-3 is significantly smaller than that of the TiO_2 sample.

3.1.4. SEM. The morphologies of the BC, TiO_2 and TBC-3 samples were analyzed by SEM (Fig. 4). Fig. 4(a)–(c) show the long-range ordered and porous structure of straw biochar, which provided a good platform for the introduction of TiO_2. Also, Fig. 4(d)–(f) demonstrate that an obvious agglomeration phenomenon occurred for pure TiO_2. Interestingly, the SEM image of BC indicates the presence of a relatively uniform and lamellar structure after loading with TiO_2, which is conducive for optimizing their respective structures [Fig. 4(g)–(i)]. The distribution of TiO_2 nanoparticles in the composites was uniform and their agglomeration was significantly reduced, implying that the presence of biochar improved the growth of TiO_2

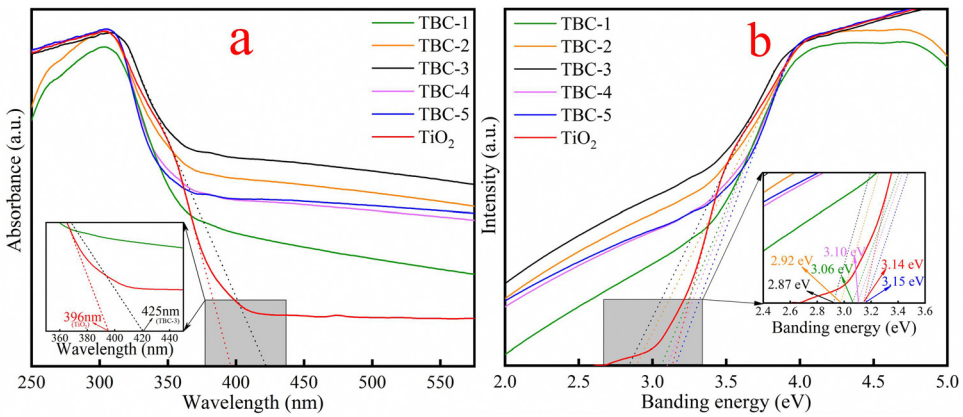

Fig. 3 UV-Vis absorption spectra (a) and corresponding band gap energies (b) of TiO_2 and TBC samples.

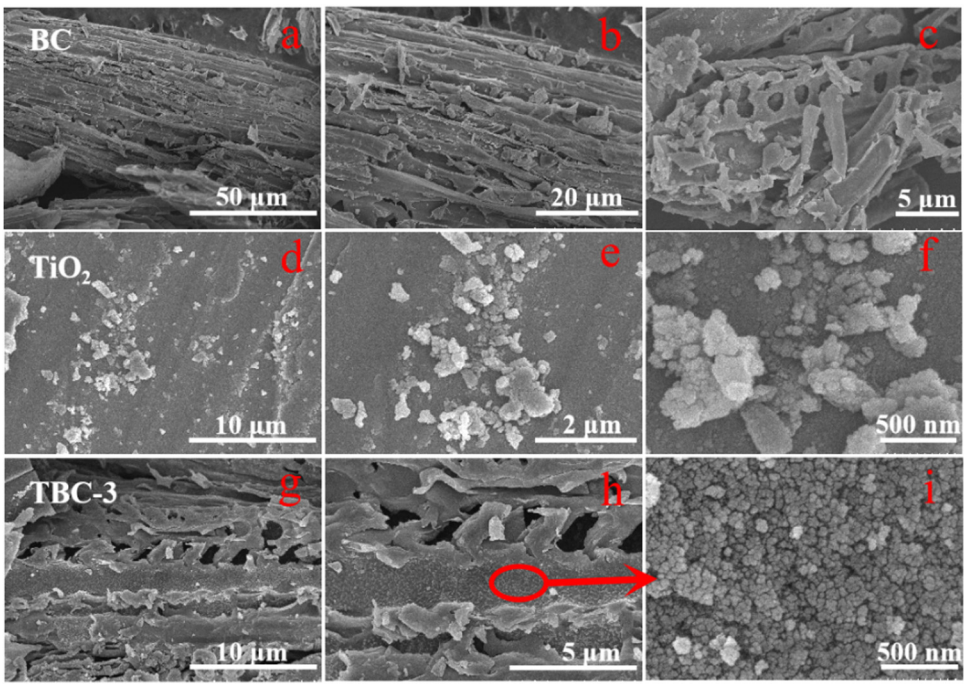

Fig. 4 Typical SEM images of the as-prepared samples. SEM images of BC (a)–(c), TiO_2 (d)–(f) and TBC-3 (g)–(i).

particles during the preparation of TiO_2 *via* the sol–gel method, as previously reported by Xie *et al.*[40]

3.1.5. TEM. The microstructure and elemental compositions of the prepared TBC-3 sample were further characterized by TEM, element mapping and EDX (Fig. 5). The high crystallization of TiO_2 with an average size of 17.4 nm was detected (Fig. 5a). Additionally, the *d*-spacing (0.36 nm) between the crystal planes corresponding to the tetragonal anatase crystal structure (101) plane was confirmed by high-resolution transmission electron microscopy (HRTEM) (Fig. 5b and c), which is consistent with the XRD results. In addition, the image of the TBC-3 sample exhibits the presence of smaller TiO_2 nanoparticles in the BC substrate, which was proven in the SEM image (Fig. 4). The element mapping images (Fig. 5d–g) revealed that the composite sample contained C, Ti and O elements and these elements were evenly distributed. The EDX pattern (Fig. 5h) and XPS data (Table S1, ESI†) reflect that the content of oxygen atoms is twice that of titanium atoms, which is basically close to the stoichiometric composition of the TiO_2 sample.

3.1.6. N_2 sorption analysis. The N_2 sorption isotherm curves and the corresponding data for the prepared BC, TiO_2 and TBC-3 composites are shown in Fig. 6 and Table S2 (ESI†). TiO_2 exhibited the typical type I isotherm, which is characteristic of microporous materials (<2 nm). In this case, the main absorption occurs at a low relative pressure, followed by an almost horizontal branch. This shape indicates a highly microporous material, which can be observed from the most probable pore size (1.75 nm) in Table S2 (ESI†). In contrast, the hysteresis loops of adsorption/desorption (H1 and H3, respectively, according to the IUPAC classification) were observed on the isotherms of the BC and TBC-3 samples, indicating that these materials have a mesoporous structure (pores with a size in the range of 2–50 nm). The hysteresis loop isotherm of BC showed no obvious saturated adsorption platform, suggesting that its pore structure is very irregular, while the hysteresis loop adsorption isotherm of the TBC-3 composite exhibited a saturated adsorption platform, which reflects that its pore size distribution is uniform. This is consistent with the SEM and TEM results. As expected, the TBC-3 composite, as shown in

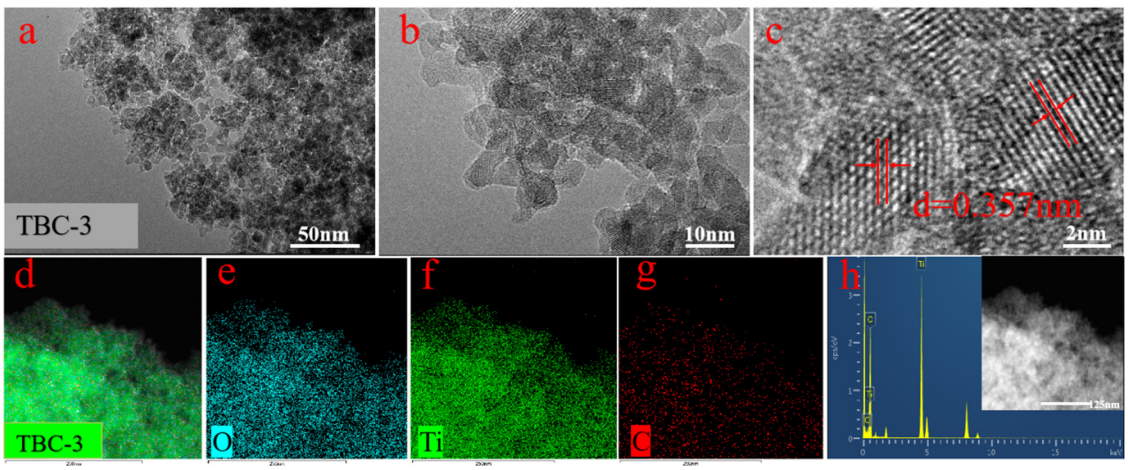

Fig. 5 Typical TEM images of the as-prepared samples. TEM images (a) and (b), HRTEM image (c), element mapping images (d)–(g) and EDX pattern (h) of the TBC-3 sample.

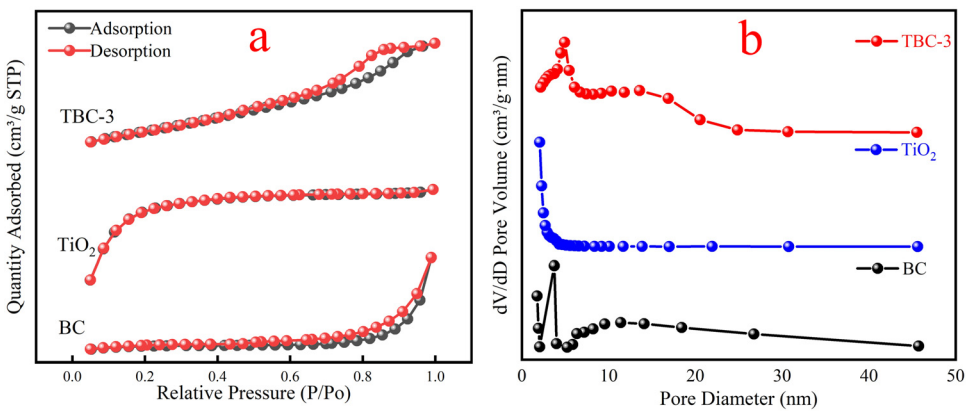

Fig. 6 Nitrogen adsorption–desorption isotherms (a) and corresponding pore size distribution curves (b) of BC, TiO_2 and TBC-3 samples.

Fig. 6a, displayed a higher adsorption capacity than that of BC and TiO_2, which also can be found from the S_{BET} data in Table S2 (ESI†). In addition, the most frequent pore diameter showed that the most widely distributed pore sizes of BC, TiO_2 and TBC-3 composites are 26.7 nm, 1.7 nm and 8.9 nm, while the pore volumes of BC and TiO_2 are 0.011 $cm^3\ g^{-1}$ and 0.065 $cm^3\ g^{-1}$, resulting in the specific surface area of the TBC-3 composite being 12.5-times and 2.5-times higher than that of BC and TiO_2, respectively. It is worth noting that compared with pure BC, the specific surface area and pore volume of the composite material are significantly higher, whereas the pore size of the composite material is smaller, reflecting that the increase in the specific surface area corresponds to the mesoporous structure. This further demonstrates the successful incorporation of TiO_2 and BC, which is consistent with the previous reports.[24,25]

3.1.7. Electrochemical analysis. Electrochemical impedance spectroscopy (EIS) measurements were performed to study the electrochemical properties of BC, TiO_2 and TBC composites, as shown in Fig. 7. The semi-circle in the Nyquist plot refers to the total impedance or charge transfer resistance at the contact interface between the working electrode coated with sample and the electrolyte solution. Generally, it is considered that the electronic conductivity of the sample is determined by the arc radius at high frequency in the EIS diagram. Specifically, the smaller the arc radius, the stronger the electronic conductivity of the as-synthesized material.[48,49] Therefore, it is obvious that the arc radius of TiO_2 was greatly reduced after loading BC, and the arc radius of the synthesized sample increased first, and then decreased with the addition of BC. Among the studied samples, the arc radius of the TBC-3 sample is the smallest, implying that its conductivity is the largest, namely, the interface separation efficiency of the TBC-3 sample is the fastest, which is consistent with the subsequent photocatalytic activity of the samples. As expected, BC has a relatively small impedance compared with the TiO_2 sample, suggesting that BC has a certain electron transport capacity and can act as an electron transfer acceptor.

3.1.8. TG analysis. Thermogravimetric analysis (TGA) was performed in an air atmosphere from 40 °C to 800 °C (see Fig. 8) to investigate the thermodynamic stability of the BC and TBC-3 samples. It can be observed that there are three stages in the BC curve. Below 300 °C, about 2.7% weight loss occurred in BC, which is ascribed to the desorption of adsorbed H_2O or air on the surface of the sample. The organic components of BC decomposed rapidly, and the weight loss rate reached as high as 63.1% from 300 °C to 550 °C. When the temperature exceeded 550 °C, the organic components of BC were almost completely decomposed, leaving only a small amount of inorganic ash and other impurities. However, in the case of the TBC-3 precursor composite, due to the loss of adsorbed water and the decomposition of titanium hydroxide to form TiO_2, its weight gradually decreased by about 15.0% when the temperature increased to 250 °C. Subsequently, there was a steep downward trend from 250 °C to 550 °C and the weight loss reached 18.0%, which may be due to the decomposition of the organic components in the BC and TiO_2 gel precursor. When the calcination temperature exceeded 550 °C, ~64.0% weight loss was observed, which is mainly ascribed to the loss of titanium dioxide and other impurities. The TGA results show that a lower calcination temperature may lead to the incomplete decomposition of titanium hydroxide. When the calcination temperature is higher than 550 °C, the organic components of BC are completely decomposed. Therefore, the optimized calcination temperature of 300 °C was selected in the experiment. This finding was supported by the following photocatalytic activity.

3.2. Adsorption-photocatalytic reduction of Cr(VI)

To explore the adsorption-photocatalytic performance of the as-prepared TBC composites, the synergistic adsorption-photocatalytic reduction experiments for Cr(VI) were carried out under simulated sunlight irradiation, and the results are shown in Fig. 9a and Fig. S1 and S2 (ESI†). The comparative

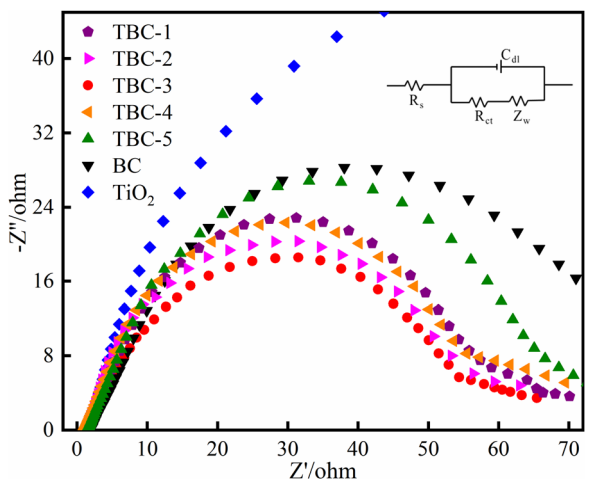

Fig. 7 EIS Nyquist plots of the as-prepared BC, TiO_2, and TBC samples in 1 M Na_2SO_4 solution and the inset shows the equivalent circuit fitting of EIS data.

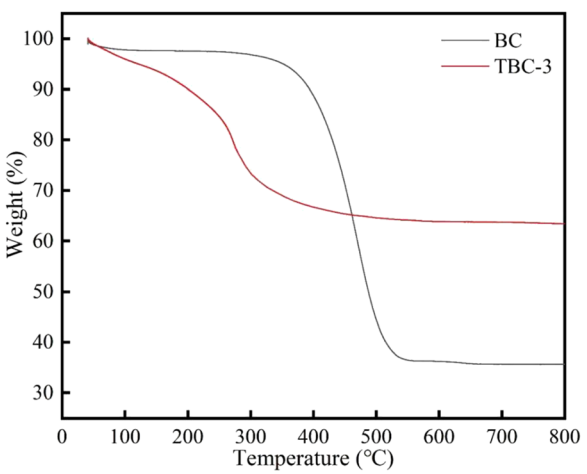

Fig. 8 TGA curves of BC and TBC-3 samples in an air atmosphere.

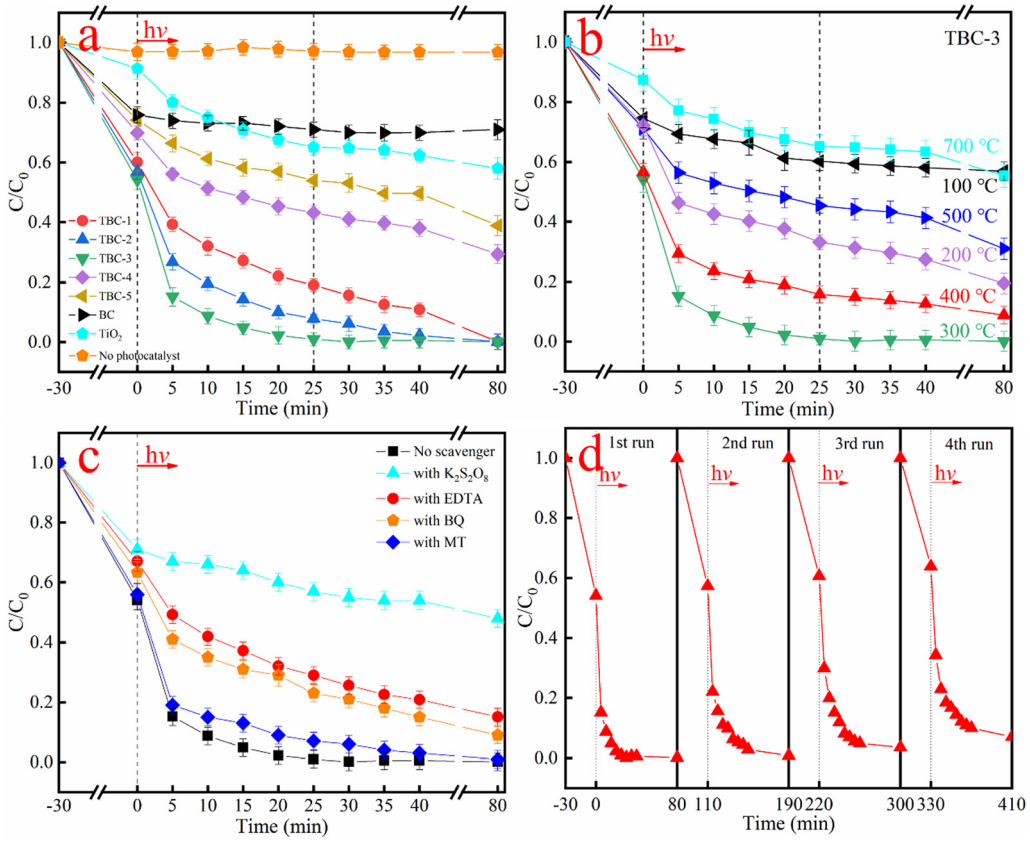

Fig. 9 Absorption-photocatalytic reduction of Cr(VI) with BC, TiO_2 and TBC samples (a), with TBC-3 calcined at different temperatures (b) and over TBC-3 composite in the presence of $K_2S_2O_8$, EDTA, BQ and MT scavengers (c). Recycling experiments using TBC-3 composite for the absorption-photocatalytic reduction of Cr(VI) (d).

experiments indicate that Cr(VI) was not basically reduced under sunlight irradiation without the addition of a photocatalyst (3.2% under sunlight irradiation for 80 min) and a certain amount of adsorption-reduction efficiency of Cr(VI) could be detected with the TBC-3 sample in the dark for 180 min (Fig. S2, ESI†), which confirms that an adsorption-photocatalytic process occurs with the TBC composites. It is clear that the adsorption efficiency of Cr(VI) for BC and the TBC composite materials after 30 min was higher than that of pure TiO_2 (only 6.1%), and the adsorption capacity increased, and then decreased in the dark, together with the decrease in the case of BC. For example, the adsorption rates of the TBC-1, TBC-2, TBC-3, TBC-4 and TBC-5 samples were about 40.2%, 42.0%, 44.1%, 30.3% and 25.2%, respectively. After sunlight illumination, the results in Fig. 9a show that the trend of adsorption-photocatalytic reduction activity for Cr(VI) also increased first, and then decreased. Among them, TBC-1, TBC-2 and TBC-3 completely adsorbed and photocatalytically reduced Cr(VI) after sunlight illumination for 70 min, 40 min and 25 min, respectively. However, TBC-4, TBC-5 and pure TiO_2 only achieved 70.3%, 60.1% and 40.3% efficiency after sunlight irradiation for 80 min, respectively. When the irradiation time was 25 min, the adsorption-photocatalytic reduction efficiencies were 81.2%, 92.4%, 99.9%, 57.0% and 46.0% for the TBC-1, TBC-2, TBC-3, TBC-4 and TBC-5 samples, while they were 34.8% and 28.9% for the TiO_2 and BC samples, respectively. Thus, the results indicate that TBC-3 showed the best performance for the adsorption-photocatalytic reduction of Cr(VI), which is approximately 2.9- and 3.5-times higher than that of the pure TiO_2 and BC samples, respectively. We also studied the XPS spectrum of Cr element on the surface of TBC-3 and in the solution after the photocatalytic reaction (Fig. S3, ESI†). The high-resolution spectrum of Cr 2p showed peaks at 577.2 and 586.5 eV, which can be ascribed to Cr $2p_{3/2}$ and Cr $2p_{1/2}$ of the Cr(III) species on the surface of TBC-3 and in solution after the photocatalytic reaction, respectively, indicating that Cr(VI) was completely reduced into Cr(III) in the presence of the TBC-3 sample under sunlight irradiation.[28] Herein, BC not only functioned as a platform for the loading of the TiO_2 photocatalyst, but also acted as a material to adsorb the target reactant. Therefore, it was concluded that TiO_2 could greatly improve the adsorption-photocatalytic efficiency for the reduction of Cr(VI) under sunlight illumination after loading of BC.

Fig. 9b displays the dependence of the adsorption-photocatalytic activity on the calcination temperature of TBC-3. It reveals that the adsorption capacity increased first, and then decreased in the dark for 30 min with an increase in the calcination temperature of TBC. According to our in-depth investigation, we found that the adsorption-photocatalytic efficiency of Cr(VI) also increased, and then decreased under

sunlight for 80 min with an increase in the calcination temperature of TBC. When the irradiation time was 25 min, the adsorption-photocatalytic efficiency for the reduction of Cr(VI) was 39.8%, 66.8%, 99.9%, 84.2%, 54.6% and 34.8% for TBC calcined at the temperature of 100 °C, 200 °C, 300, 400 °C, 500 °C and 700 °C, respectively, which exhibits that the optimal composite material is TBC-3 calcined at 300 °C. This observation can be interpreted as follows. When the calcination temperature is too low or too high, BC is encapsulated in unhydrolyzed tetrabutyl titanate or will be burned and decomposed, finally affecting its adsorption and photocatalytic capacity.

To study the reaction mechanism, the adsorption-photocatalytic reduction of Cr(VI) by the composite material was performed in the presence of a series of sacrificial agents (Fig. 9c). Potassium persulfate ($K_2S_2O_8$), methanol (MT), ethylenediaminetetraacetic acid (EDTA), and benzoquinone (BQ) (1 M each) were used as scavengers for e^-, h^+, $OH^{\bullet-}$, and $O_2^{\bullet-}$, respectively.[50] When $K_2S_2O_8$ was added to the reaction system, the synergistic adsorption-photocatalytic efficiency for the reduction of Cr(VI) decreased significantly to 32.0% under sunlight irradiation for 80 min, indicating that electrons (e^-) played a major role during the photocatalytic process. However, when the sacrificial agents were MT, EDTA and BQ, the adsorption-photocatalytic efficiency reached 100%, 78.3% and 88.9% under sunlight irradiation for 80 min, reflecting that h^+, $OH^{\bullet-}$ and $O_2^{\bullet-}$ are not important active species in the photocatalytic reaction, respectively. It is noteworthy that the composite material is composed of an adsorbent material and photocatalyst. The surface area and porosity of the adsorbent/photocatalyst composite affect the "adsorption and shuttle" process, which further enhances the photocatalytic removal rate of Cr(VI).[51] This is because the "adsorption and shuttle" is related to the use of the structure of the adsorption material to increase the type and quantity of pollutants near the photocatalytic site of TiO_2, thereby significantly improving the photocatalytic efficiency of TiO_2.[52]

In practical applications, the reusability and chemical stability of a photocatalyst are crucial factors. Hence the adsorption-photocatalytic reduction of Cr(VI) with the TBC-3 photocatalyst was investigated. The experimental tests lasted for a total of 320 min, and after every 80 min of reaction, the used TBC-3 sample was washed with deionized water several times, dried at 60 °C for 12 h, and then re-dispersed in a new reaction system. The experimental results are displayed in Fig. 9d. Under absorption and sunlight irradiation, there was no significant change in the activity after 4 repeated cycles, which suggests that the TBC-3 photocatalyst has excellent chemical stability under sunlight irradiation.

The photocatalytic activities and the corresponding zeta potentials of the TBC-3 sample at different solution pH values were also examined, as shown in Fig. S4 and S5 (ESI†). It is obvious that the photocatalytic performance of the TBC-3 sample was severely affected by the solution pH value. Moreover, with an increase in the pH value, the photocatalytic activity increased, and then decreased. For example, under sunlight irradiation for 25 min, the adsorption-photocatalytic efficiencies for the reduction of Cr(VI) were 85.4%, 99.9%, 72.6%, 70.0% and 36.8% with TBC-3 at pH 1.4, 3.1, 5.1, 7.0 and 9.1, respectively. This can be explained by the zeta potential of the TBC-3 sample at different solution pH values. When the pH was 3.1, a more positive zeta potential value was observed for the TBC-3 sample among the studied pH values. Therefore, a more positive charge surface is beneficial for the process of Cr(VI) absorption and Cr(III) desorption during the reaction process, finally improving the photocatalytic reduction performance.[53]

3.3. Reaction mechanism

Based on the above-mentioned analysis, the significantly enhanced efficiency of the TBC composites for the absorption-photocatalytic reduction of Cr(VI) under sunlight illumination can mainly be attributed to the addition of BC as well as the intimate interfacial contact between BC and TiO_2. Thereby, the potential reaction mechanism for the absorption-photocatalytic reduction of Cr(VI) on the TBC composites under sunlight illumination is proposed, as displayed in Scheme 1. Under sunlight irradiation, photogenerated carriers are produced on the surface of the TiO_2 sample, and then the photogenerated electrons are promoted to the conduction band (CB), leaving holes in the valence band (VB). After loading BC with high conductivity and adsorption capacity, the excited electrons spontaneously migrate to the surface of BC, which is conducive to the spatial separation of the photoexcited electron–hole pairs. Subsequently, the photoexcited electrons with moderate reduction ability can reduce Cr(VI) to Cr(III), as well as the photoexcited holes are trapped and reacted with methanol. It has been reported that the C=O and O=C–OH groups of BC can play a similar role as noble metals and electron-acceptor molecules deposited on the surface of semiconductors.[54]

4. Conclusions

In summary, a series of TBC composite materials was prepared by a simple multiple-calcination method. Their adsorption-photocatalytic performance was evaluated by the adsorption-

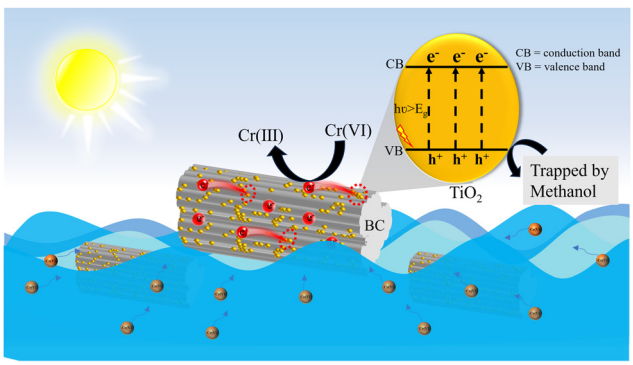

Scheme 1 Proposed mechanism for the synergistic effect of adsorption-photocatalytic reduction of Cr(VI) on TBC composite under sunlight irradiation.

photocatalytic reduction of Cr(VI) to the nontoxic Cr(III) under simulated sunlight irradiation. The results indicate that the adsorption-photocatalytic reduction efficiency of Cr(VI) obviously improved after loading BC derived from agricultural biomass waste. Further research exhibited that the adsorption-photocatalytic reduction efficiency of Cr(VI) increased, and then decreased with the loading amount of BC, and the optimized TBC-3 composite showed the highest adsorption-photocatalytic efficiency for the reduction of Cr(VI) ($\sim$99.9%) under sunlight irradiation for 25 min, which is *ca.* 2.9 and 3.5 times higher than that of the pure TiO_2 and BC samples, respectively. The outstanding adsorption-photocatalytic efficiency for the reduction of Cr(VI) was ascribed to the synergistic effect of the strong adsorption of BC and the superior photocatalytic reduction ability of TiO_2. Finally, the possible synergistic effect for the adsorption-photocatalytic reduction of Cr(VI) with TBC-3 under sunlight illumination was proposed. This work paves a new path for the development of new and efficient biochar-based composite materials with potential applications in the treatment of highly toxic chromium-containing wastewater.

Conflicts of interest

There are no conflicts to declare.

Acknowledgements

This work was supported by the Natural Science Foundation of Anhui Province (Nos. 2022AH051625, 2008085MC81, 2022AH051655 and 202004a06020003), Young and Middle-aged Subject Leaders of Anhui Science and Technology University (No. 210011), The University-Industry Collaboration Program with Anhui Haohong Biotechnology Co., Ltd. (No. 881351), Enterprise Horizontal Project Fund (No. 2020QX001) and Anhui Young Scholars Project (No. 000012).

References

1 J. P. Wise, J. L. Young, J. Cai and L. Cai, Current understanding of hexavalent chromium [Cr(VI)] neurotoxicity and new perspectives, *Environ. Int.*, 2022, **158**, 106877.
2 P. Sharma, S. P. Singh, S. K. Parakh and Y. W. Tong, Health hazards of hexavalent chromium (Cr(VI)) and its microbial reduction, *Bioengineered*, 2022, **13**, 4923–4938.
3 K. E. Ukhurebor, U. O. Aigbe, R. B. Onyancha, W. Nwankwo, O. A. Osibote, H. K. Paumo, O. M. Ama, C. O. Adetunji and I. U. Siloko, Effect of hexavalent chromium on the environment and removal techniques: A review, *J. Environ. Manage.*, 2021, **280**, 111809.
4 C. Y. Hu, S. L. Lo, Y. H. Liou, Y. W. Hsu, K. Shih and C. J. Lin, Hexavalent chromium removal from near natural water by copper-iron bimetallic particles, *Water Res.*, 2010, **44**, 3101–3108.
5 G. Zhang, T. Ge, Y. Zhang and E. Zhang, Hydrothermal preparation of Nb^{5+}-doped α-Fe_2O_3 nanorods for efficient visible light-driven photocatalytic reduction of hexavalent chromium, *Powder Technol.*, 2024, **436**, 119480.
6 Z. Jiang, K. Chen, Y. Zhang, Y. Wang, F. Wang, G. Zhang and D. D. Dionysiou, Magnetically recoverable $MgFe_2O_4$/conjugated polyvinyl chloride derivative nano-composite with higher visible-light photocatalytic activity for treating Cr(VI)-polluted water, *Sep. Purif. Technol.*, 2020, **236**, 116272.
7 F. Djouider, Radiolytic formation of non-toxic Cr(III) from toxic Cr(VI) in formate containing aqueous solutions: A system for water treatment, *J. Hazard. Mater.*, 2012, **223–224**, 104–109.
8 X. Zhou, T. Korenaga, T. Takahashi, T. Moriwake and S. Shinoda, A process monitoring/controlling system for the treatment of wastewater containing chromium(VI), *Water Res.*, 1993, **27**, 1049–1054.
9 S. Rengaraj, C. K. Joo, Y. Kim and J. Yi, Kinetics of removal of chromium from water and electronic process wastewater by ion exchange resins: 1200H, 1500H and IRN97H, *J. Hazard. Mater.*, 2003, **102**, 257–275.
10 E. Korngold, N. Belayev and L. Aronov, Removal of chromates from drinking water by anion exchangers, *Sep. Purif. Technol.*, 2003, **33**, 179–187.
11 A. K. Sengupta, D. Clifford and S. Subramonian, Chromate ion-exchange process at alkaline pH, *Water Res.*, 1986, **20**, 1177–1184.
12 L. Alvarado, A. Ramírez and I. Rodríguez-Torres, Cr(VI) removal by continuous electrodeionization: Study of its basic technologies, *Desalination*, 2009, **249**, 423–428.
13 A. Tor, T. Büyükerkek, Y. Çengelolu and M. Ersöz, Simultaneous recovery of Cr(III) and Cr(VI) from the aqueous phase with ion-exchange membranes, *Desalination*, 2005, **171**, 233–241.
14 H. Hsu, S. Chen and Y. Chen, Removal of chromium(VI) and naphthalenesulfonate from textile wastewater by photocatalysis combining ionic exchange membrane processes, *Sep. Purif. Technol.*, 2011, **80**, 663–669.
15 N. N. Fathima, R. Aravindhan, J. R. Rao and B. U. Nair, Solid waste removes toxic liquid waste: Adsorption of chromium(VI) by iron complexed protein waste, *Environ. Sci. Technol.*, 2005, **39**, 2804–2810.
16 Y. Xing, X. Chen and D. Wang, Electrically regenerated ion exchange for removal and recovery of Cr(VI) from wastewater, *Environ. Sci. Technol.*, 2007, **41**, 1439–1443.
17 J. C. Almeida, C. E. D. Cardoso, D. S. Tavares, R. Freitas, T. Trindade, C. Vale and E. Pereira, Chromium removal from contaminated waters using nanomaterials-A review, *Trends Anal. Chem.*, 2019, **118**, 277–291.
18 N. Abdollahi, G. Moussavi and S. Giannakis, A review of heavy metals' removal from aqueous matrices by Metal-Organic Frameworks (MOFs): State-of-the art and recent advances, *J. Environ. Chem. Eng.*, 2022, **10**, 107394.
19 W. Wang and A. Wang, Perspectives on green fabrication and sustainable utilization of adsorption materials for wastewater treatment, *Chem. Eng. Res. Des.*, 2022, **187**, 541–548.
20 Q. Zhang, J. Wang, X. Ye, Z. Hui, L. Ye, X. Wang and S. Chen, Self-assembly of $CdS/CdIn_2S_4$ heterostructure with

enhanced photocascade synthesis of Schiff base compounds in an aromatic alcohols and nitrobenzene system with visible light, *ACS Appl. Mater. Interfaces*, 2019, **11**, 46735–46745.

21 Z. Xing, J. Zhang, J. Cui, J. Yin, T. Zhao, J. Kuang, Z. Xiu, N. Wan and W. Zhou, Recent advances in floating TiO_2-based photocatalysts for environmental application, *Appl. Catal., B*, 2018, **225**, 452–467.

22 H. Tong, S. Ouyang, Y. Bi, N. Umezawa, M. Oshikiri and J. Ye, Nano-photocatalytic materials: Possibilities and challenges, *Adv. Mater.*, 2012, **24**, 229–251.

23 D. Hao, Q. Huang, W. Wei, X. J. Bai and B.-J. Ni, A reusable, separation-free and biodegradable calcium alginate/g-C_3N_4 microsphere for sustainable photocatalytic wastewater treatment, *J. Clean. Prod.*, 2021, **314**, 128033.

24 R. Djellabi, B. Yang, Y. Wang, X. Cui and X. Zhao, Carbonaceous biomass-titania composites with Ti–O–C bonding bridge for efficient photocatalytic reduction of Cr(VI) under narrow visible light, *Chem. Eng. J.*, 2019, **366**, 172–180.

25 H. Zakaria, Y. Li, M. M. Fathy, X. Zhou, X. Xiong, Y. Wang, S. Rong and C. Zhang, A novel TiO_{2-X}/TiN@ACB composite for synchronous photocatalytic Cr(VI) reduction and water photothermal evaporation under visible/infrared light illumination, *Chemosphere*, 2022, **311**, 137137.

26 G. P. Zhang, D. Y. Chen, N. J. Li, Q. F. Xu, H. Li, J. H. He and J. M. Lu, Preparation of $ZnIn_2S_4$ nanosheet-coated CdS nanorod heterostructures for efficient photocatalytic reduction of Cr(VI), *Appl. Catal., B*, 2018, **232**, 164–174.

27 M. H. Li, W. J. Liu, P. X. Liu, X. Q. Lin, H. J. Zhu, C. X. Fang, W. W. Li and C. Liu, Engineering Fe-N-C sites onto Fe nanoparticles for synergistically boosting Cr(VI) reduction: performance, mechanism, and applications, *J. Mater. Chem. A*, 2024, **12**, 7817.

28 J. H. Zheng and L. Zhang, Incorporation of CoO nanoparticles in 3D marigold flower-like hierarchical architecture $MnCo_2O_4$ for highly boosting solar light photo-oxidation and reduction ability, *Appl. Catal., B*, 2018, **237**, 1–8.

29 J. Yang, Y. J. Liang, K. Li, G. Yang and S. Yin, One-step low-temperature synthesis of 0D CeO_2 quantum dots/2D BiOX (X = Cl, Br) nanoplates heterojunctions for highly boosting photo-oxidation and reduction ability, *Appl. Catal., B*, 2019, **250**, 17–30.

30 J. Schneider, M. Matsuoka, M. Takeuchi, J. Zhang, Y. Horiuchi, M. Anpo and D. W. Bahnemann, Understanding TiO_2 photocatalysis: Mechanisms and materials, *Chem. Rev.*, 2014, **114**, 9919–9986.

31 Y. C. Zhang, M. Yang, G. Zhang and D. D. Dionysiou, HNO_3-involved one-step low temperature solvothermal synthesis of N-doped TiO_2 nanocrystals for efficient photocatalytic reduction of Cr(VI) in water, *Appl. Catal., B*, 2013, **142–143**, 249–258.

32 S. Malato, P. Fernández-Ibáñez, M. I. Maldonado, J. Blanco and W. Gernjak, Decontamination and disinfection of water by solar photocatalysis: Recent overview and trends, *Catal. Today*, 2009, **147**, 1–59.

33 K. S. Divya, M. M. Xavier, P. V. Vandana, V. N. Reethu and S. Mathew, A quaternary TiO_2/ZnO/RGO/Ag nanocomposite with enhanced visible light photocatalytic performance, *New J. Chem.*, 2017, **41**, 6445–6454.

34 Z. L. Liu, C. Zhang, L. Z. Liu, T. S. Zhang, J. Wang, R. Wang, T. Du, C. Y. Yang, L. Zhang, L. X. Xie, W. X. Zhu, T. L. Yue and J. L. Wang, A conductive network and dipole field for harnessing photogenerated charge kinetics, *Adv. Mater.*, 2021, **33**, 2104099.

35 S. B. Kim, S.-Y. Lee and S.-J. Park, TiO_2/Multi-walled carbon nanotube electrospun nanofibers mats for enhanced Cr(VI) photoreduction, *J. Clean. Prod.*, 2024, **448**, 141611.

36 Q. Huang, S. Song, Z. Chen, B. Hu, J. Chen and X. Wang, Biochar-based materials and their applications in removal of organic contaminants from wastewater: State-of- the-art review, *BioChar*, 2019, **1**, 45–73.

37 S. Ye, M. Yan, X. Tan, J. Liang, G. Zeng, H. Wu, B. Song, C. Zhou, Y. Yang and H. Wang, Facile assembled biochar-based nanocomposite with improved graphitization for efficient photocatalytic activity driven by visible light, *Appl. Catal., B*, 2019, **250**, 78–88.

38 Z. Jin, S. Xiao, H. Dong, J. Xiao, R. Tian, J. Chen, Y. Li and L. Li, Adsorption and catalytic degradation of organic contaminants by biochar: Overlooked role of biochar's particle size, *J. Hazard. Mater.*, 2022, **422**, 126928.

39 L. Chen, S. Yang, X. Zuo, Y. Huang, T. Cai and D. Ding, Biochar modification significantly promotes the activity of Co_3O_4 towards heterogeneous activation of peroxymonosulfate, *Chem. Eng. J.*, 2018, **354**, 856–865.

40 X. Xie, S. Li, H. Zhang, Z. Wang and H. Huang, Promoting charge separation of biochar-based Zn-TiO_2/pBC in the presence of ZnO for efficient sulfamethoxazole photodegradation under visible light irradiation, *Sci. Total Environ*, 2019, **659**, 529–539.

41 H. Huang, Y. Wang, W. Jiao, F. Cai, M. Shen, S. Zhou, H. Cao, J. Lü and R. Cao, Lotus-leaf-derived activated-carbon-supported nano-CdS as energy-efficient photo- catalysts under visible irradiation, ACS Sustain, *Chem. Eng.*, 2018, **6**, 7871–7879.

42 L. Lu, R. Shan, Y. Shi, S. Wang and H. Yuan, A novel TiO_2/biochar composite catalysts for photocatalytic degradation of methyl orange, *Chemosphere*, 2019, **222**, 391–398.

43 M. M. Mian and G. Liu, Recent progress in biochar-supported photocatalysts: synthesis, role of biochar, and applications, *RSC Adv.*, 2018, **8**, 14237–14248.

44 M. Pettine and S. Capri, Removal of humic matter interference in the determination of Cr(VI) in soil extracts by the diphenylcarbazide method, *Anal. Chim. Acta*, 2005, **540**, 239–246.

45 Y. Guo, T. Guo, J. Chen, J. Wei, L. Bai, X. Ye, Z. Ding, W. Xu and Z. Zhou, Synthesis of C-N-S co-doped TiO_2 mischcrystal with an isobandgap characteristic and its photocatalytic activity under visible light, *Catal. Sci. Technol.*, 2018, **8**, 4108–4121.

46 D. Chen, Z. Jiang, J. Geng, Q. Wang and D. Yang, Carbon and nitrogen Co-doped TiO_2 with enhanced visible-light photocatalytic activity, *Ind. Eng. Chem. Res.*, 2007, **46**, 2741–2746.

47 Y. Zhang, C. Liu, P. Nian, H. Ma, J. Hou and Y. Zhang, Facile preparation of high- performance hydrochar/TiO_2 heterojunction visible light photocatalyst for treating Cr(VI)-polluted water, *Colloids Surf., A*, 2024, **681**, 132775.

48 X. Ye, Y. Chen, C. Ling, J. Zhang, S. Meng, X. Fu, X. Wang and S. Chen, Chalcogenide photocatalysts for selective oxidation of aromatic alcohols to aldehydes using O_2 and visible light: A case study of $CdIn_2S_4$, CdS and In_2S_3, *Chem. Eng. J.*, 2018, **348**, 966–977.

49 Y. Zhang, F. Zhang, Z. Yang, H. Xue and D. D. Dionysiou, Development of a new efficient visible-light-driven photocatalyst from SnS_2 and polyvinyl chloride, *J. Catal.*, 2016, **344**, 692–700.

50 S. Y. Chen, J. P. Yu, Z. F. Chai, W. Q. Shi and L. Y. Yuan, Is the sacrificial agent really just a sacrificial agent? A case study on the photocatalytic reduction of U(VI) by alcohols, *Chem. Eng. J.*, 2023, **460**, 141742.

51 R. Djellabi, M. F. Ghorab, G. Cerrato, S. Morandi, S. Gatto, V. Oldani, A. Di Michele and C. L. Bianchi, Photoactive TiO_2-montmorillonite composite for degradation of organic dyes in water, *J. Photochem. Photobiol., A*, 2014, **295**, 57–63.

52 S. MiarAlipour, D. Friedmann, J. Scott and R. Amal, TiO_2/porous adsorbents: Recent advances and novel applications, *J. Environ. Manage.*, 2018, **341**, 404–423.

53 Z. Fang, Q. Li, L. Su, J. H. Chen, K.-C. Chou and X. M. Hou, Efficient synergy of photocatalysis and adsorption of hexavalent chromium and rhodamine B over Al_4SiC_4/rGO hybrid photocatalyst under visible-light irradiation, *Appl. Catal., B*, 2019, **241**, 548–560.

54 Y. Wang, Z. Ao, H. Sun, X. Duan and S. Wang, Activation of peroxymonosulfate by carbonaceous oxygen groups: Experimental and density functional theory calculations, *Appl. Catal., B*, 2016, **198**, 295–302.